Agricultural and Forest Meteorology 268 (2019) 169–180

Contents lists available at ScienceDirect

Agricultural and Forest Meteorology

journal homepage: www.elsevier.com/locate/agrformet

The biophysical effects of the vegetation restoration program on regional climate metrics in the Loess Plateau, China

Qian Cao[a], Jianguo Wu[a,b], Deyong Yu[a,*], Wei Wang[c]

[a] Center for Human-Environment System Sustainability (CHESS), State Key Laboratory of Earth Surface Processes and Resource Ecology, College of Natural Resources, Faculty of Geographical Science, Beijing Normal University, Beijing, 100875, China
[b] School of Life Sciences and School of Sustainability, Arizona State University, Tempe, AZ, 85287, United States
[c] Mesoscale & Microscale Meteorology Laboratory, National Center for Atmospheric Research (NCAR), Boulder, CO, 80301, United States

ARTICLE INFO

Keywords:
The Grain to Green program
Afforestation
Vegetation characteristics
Land use/land cover
Land-atmosphere interaction
WRF

ABSTRACT

The Grain to Green (GTG) program launched in 1999 by the Chinese government is one of the largest ecological restoration programs ever implemented in the world. Although the GTG program has been demonstrated to affect ecosystem services in the revegetated areas, its impacts on regional climate are seldom reported and poorly understood. Therefore, our study examined the impacts of revegetation owing to the GTG program on summer climate in the Loess Plateau, by incorporating near real-time remotely sensed land use/land cover data and vegetation characteristics of 2001 and 2010 into a coupled land-atmosphere model. From 2001 to 2010, a considerable portion of croplands was converted to forests and grasslands, with vegetation fraction and LAI increasing while surface albedo decreasing throughout the Loess Plateau. Compared with those from 2001, simulation results from 2010 indicated lowered 2-m air temperature in summer, with the magnitude of reduction in nighttime minimum (as high as 0.8–1.0 ℃) greater than that in daytime maximum (generally restricted to 0.4 ℃). The concurrent decrease in summertime 2-m specific humidity further led to widespread reduction of near-surface heat content (i.e., moist enthalpy). Summer precipitation decreased in northern Shanxi province and western Loess Plateau (up to 1.0–1.4 mm/day) while increasing in southeastern Loess Plateau (between 1.0–2.0 mm/day). Our findings underscore that vegetation restoration has exerted strong influences on regional climate, and provide useful information for the sustainable implementation of the GTG program.

1. Introduction

The Grain to Green (GTG) program, launched in 1999 by the Chinese government, is perhaps the largest ecological restoration and rural development program ever implemented on Earth (Bryan et al., 2018). By returning cultivated lands to forests and grasslands, the GTG program is proposed to restore degraded ecosystems in western China, where drought, sandstorm, and flood as a consequence of severe soil erosion have greatly threatened the lives and properties of local residents. Up to 2010, as much as 31 billion USD has been invested to the GTG program and nearly 28% of the total amount of capital has been flowed to the Loess Plateau (Feng et al., 2016), the most widely distributed and highly erodible loessal areas of the world. Previous research, based on satellite-derived vegetation characteristics (e.g., NDVI, leaf area index, and surface albedo), has shown that the Loess Plateau experienced the most significant increases in greenness across mainland China during 2000–2010, and such changes were primarily caused by human activities (Xiao, 2014; Fan et al., 2015a; Zhai et al., 2015; Li et al., 2017).

The dramatic vegetation changes due to the GTG program and the subsequent environmental outcomes have received great attention in the geographical and ecological communities. Recent studies have reported considerable increases in the net primary productivity (NPP) in the Loess Plateau, along with increasing carbon sequestration and reducing sediment export to the Yellow River (Feng et al., 2013; Su and Fu, 2013; Wang et al., 2016). Meanwhile, researchers also argued that revegetation in this semi-arid region may give rise to water shortage because of increased evapotranspiration (Chen et al., 2015; Feng et al., 2016; Li et al., 2016). Therefore, tradeoffs between water yield and sediment control exist (Su and Fu, 2013), and additions to NPP should not exceed a certain threshold so as to maintain a sustainable human-environment system (Feng et al., 2016). Undoubtedly, these debates give valuable insights into the impacts of the GTG program on ecosystem services and provide useful information on policy making.

* Corresponding author at: No. 19 XinJieKouWai Street, Beijing, 100875, China.
E-mail address: ydy@bnu.edu.cn (D. Yu).

https://doi.org/10.1016/j.agrformet.2019.01.022
Received 11 October 2018; Received in revised form 15 January 2019; Accepted 17 January 2019

However, additional long-term, large-scale climate effects of landscape changes induced by the vegetation restoration program may also be occurring.

Landscape changes, including alterations to land use/land cover categories and land surface biophysical properties, have been recognized to be a highly significant driver of regional climate change (Feddema et al., 2005; Foley et al., 2005; Pielke, 2005). Landscape changes can affect climate through two general pathways: biogeochemical and biogeophysical (Feddema et al., 2005). The biogeochemical processes by altering the chemical composition of the atmosphere have been well established and included, though to some extent, in the IPCC assessment reports (e.g., deforestation is considered through emission scenarios of CO_2; Pielke et al., 2011). However, the biogeophysical processes can lead to climate change of similar, or greater, magnitude as effects owing to greenhouse gas emissions (Pitman et al., 2012; Georgescu et al., 2014). By modification of land surface biophysical properties (e.g., vegetation fraction, leaf area index, and surface albedo), the biogeophysical pathway can directly affect the transport of heat, moisture, and momentum between the land surface and overlying atmosphere, thus resulting in temperature, air circulation as well as precipitation changes (Pielke and Niyogi, 2009).

Although the effects of the GTG program on regional climate in the revegetated areas have yet to be adequately understood, emerging interest in understanding that has been found recently (e.g., Fan et al., 2015a, b; Li et al., 2015; Wang et al., 2018). As a step forward, Fan et al. (2015b) used the attribution analysis to evaluate the contribution of vegetation changes during 2001–2009 to climate change in the Loess Plateau, and found that background climate variations exerted larger influences on surface air temperature than vegetation changes did, while human activities had greater impacts on precipitation in the arid north than the humid south of the region. This work makes an initial and beneficial attempt to qualitatively assess climate responses to the GTG program in the policy-implemented areas. However, as stated in Fan et al. (2015a), the feedback from vegetation to the climate system is complicated and cannot be easily distinguished from background climate conditions when only examining meteorological observations. That is, process-based modeling approaches to quantitatively characterize the spatiotemporal patterns and physical drivers of regional climate change associated with the GTG program are necessary.

With the above issues in mind, we therefore apply the Weather Research and Forecasting (WRF) model (Skamarock et al., 2008) to evaluate the effects of vegetation restoration on regional climate over the Loess Plateau, a place that has experienced a series of government-supported ecological restoration programs since 1980s (Liu et al., 2017). To our knowledge, this is the first research to quantify the biogeophysical feedback of the GTG program to regional climate. We parametrize the WRF model by using satellite-estimated landscape representation (i.e., land use/land cover type, vegetation fraction, leaf area index, and surface albedo) corresponding to 2001 and 2010, respectively, so as to assess climate responses to vegetation changes induced by the implementation of the GTG program in the first decade. We seek to answer the following questions: 1) Did the GTG program result in considerable vegetation changes in the Loess Plateau between 2001 and 2010? 2) Did these vegetation changes have any major effects on regional climate metrics (e.g., 2-m air temperature, humidity, and precipitation)? 3) What are the implications of our findings for the GTG program?

2. Study area

The Loess Plateau is located in the middle reaches of the Yellow River in northern China (Fig. 1). With an area of ~ 640,000 km^2, the Loess Plateau ranks as the third largest plateau across China (following the Tibetan Plateau and Inner Mongolian Plateau) and the first largest loess plateau around the world. It covers almost all of the provinces of Shaanxi and Shanxi and extends into parts of Gansu, Ningxia, Inner Mongolia, Qinghai, and Henan. The elevation here can vary widely from 800 to 3000 m with landscapes carved by rivers rushing deep underground. The Loess Plateau is characterized by a temperate continental climate regime with intra-annul temperature ranging between 4–14 ℃ and precipitation between 200–750 mm (Su and Fu, 2013). About 60–70% of the total annual precipitation drops from June to September. The region spans three climate zones from south to north: semi-humid, semi-arid, and arid.

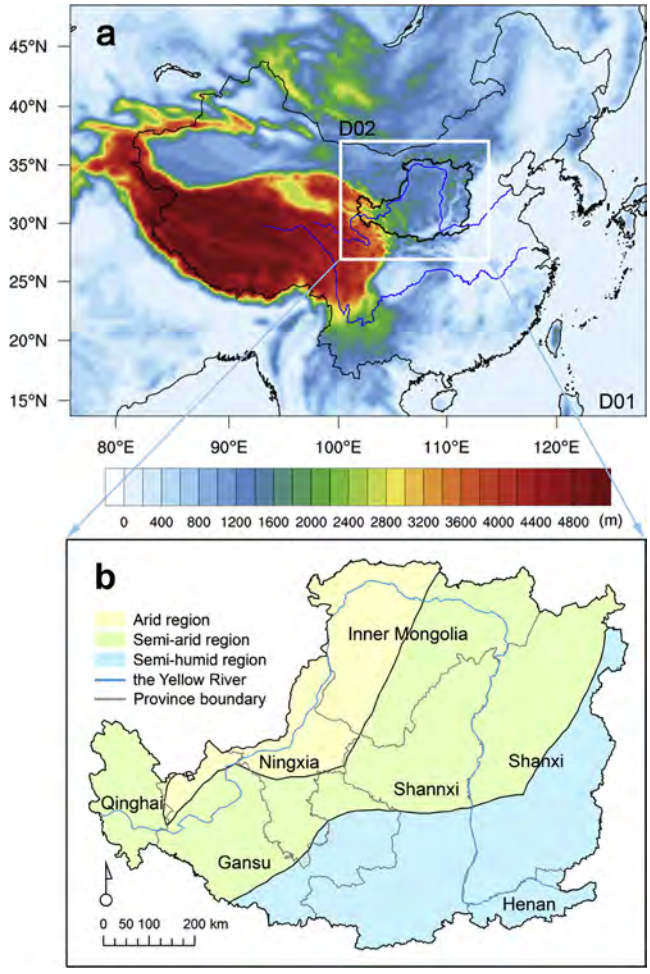

Fig. 1. Illustration of the model domain used in the WRF simulations with topography overlaid (a; unit: m) and division of climate zones in the Loess Plateau with administrative boundaries underlaid (b).

The natural vegetation in the Loess Plateau should be dominated by grasslands and forest steppe (Shang and Li, 2010). However, centuries of overuse (e.g., reclamation and overgrazing) led to one of the highest erosion rates on the planet (Wang et al., 2010). By 2000, farmlands had accounted for ~ 36% of the total land areas in this region owing to the high population growth rate. With the goal of returning regions like the Loess Plateau to more sustainable environmental conditions, the Chinese government has implemented a series of ecological restoration programs since 1980s, with the GTG program launched in 1999 being the largest and most influential one (Bryan et al., 2018). As a result, the Loess Plateau has undergone substantial increments of greenness in recent decades (see a view of Wuqi county in Yan'an city, Shaanxi province in Fig. 2), with dramatic improvements on its environmental conditions (Liu et al., 2017).

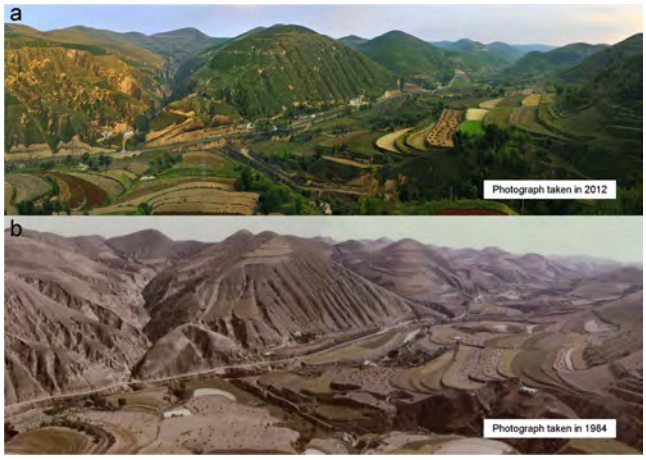

Fig. 2. A view of Wuqi county in Yan'an city, Shaanxi province during summer: (a) photograph taken in 2012 and (b) photograph taken in 1984 (http://www.xinhuanet.com/). Both photographs are in true color.

3. Materials and methods

3.1. Model configuration and parameterization

Simulations were performed using the Weather Research and Forecasting (WRF) model with the advanced dynamic solver version 3.8.1 (Skamarock et al., 2008). The WRF model was configured with two-way double nested model domains having grid spacing of 30 km and 10 km, respectively, in both horizontal directions (Fig. 1). The outer domain, D01, covered the entirety of China (including the Tibetan Plateau) and the Mongolian Plateau while extending into portions of the East and South China Sea, with a total area of 5850 km × 4200 km. This domain was sufficiently expansive to capture the influence of topography and monsoon circulation on the climate of the Loess Plateau (Wang et al., 2018). The inner domain, D02, was centered on the Loess Plateau and enclosed an area of 1500 km × 1200 km. A Lambert conformal conic projection was utilized for the model's horizontal coordinate and the model's vertical coordinate employed 45 terrain-following eta levels from the surface to 50 hPa. The initial and lateral boundary conditions for large-scale atmospheric fields were provided by the National Centers for Environmental Prediction (NCEP) through the Global Final Analysis (FNL) data archive (http://rda.ucar.edu/), with a 6-h temporal frequency and 1° grid spacing in x- and y-directions.

The main physical parameterizations used for all simulations are presented in Table 1. The multi-scale Kain-Fritsch cumulus convective scheme with scale-dependent dynamic adjustment timescale was chosen to improve the accuracy of simulated high-resolution (1–10 km) precipitation (Zheng et al., 2016). Furthermore, the subgrid-scale cloud-radiation interaction was turned on to generate more realistic longwave and shortwave radiation variability (Zheng et al., 2016). In order to represent land surface processes, the Noah land surface model (LSM; Chen and Dudhia, 2001) coupled with the WRF model was used to simulate the energy, moisture, and momentum exchange between the land surface and overlying atmosphere. Although the coupled WRF-Noah LSM has been widely applied to simulating land-atmosphere interactions, deficiencies exist with its prescribed vegetation characteristics (Cao et al., 2015). Therefore, we used the newly developed satellite-derived land surface products with detailed biophysical information to improve characterization of landscapes in the coupled model, and most importantly, to represent changes in land surface biophysical parameters due to the GTG program in the Loess Plateau.

Table 1
Main physical parameterizations used for all simulations.

Model version:	Version 3.8.1
Horizontal grid (innermost):	ΔX and ΔY = 10 km
Number of points (innermost):	150 (X direction), 120 (Y direction)
Vertical levels:	45 levels
Time step (innermost):	50 seconds
Radiation scheme:	RRTMG[a] (longwave and shortwave)
Land surface model:	Noah LSM
Cumulus scheme:	Multi-scale Kain-Fritsch (turned on)
Microphysics scheme:	WSM-3[b]
PBL scheme:	YSU[c]
Surface layer:	MM5 similarity[d]
Initial/lateral boundary conditions:	NCEP FNL

[a] RRTMG, a new version of the Rapid Radiative Transfer Model (RRTM).
[b] WSM-3, the WRF Single-Moment 3 class microphysics scheme.
[c] YSU, the Yonsei University planetary boundary layer (PBL) scheme.
[d] MM5 similarity, the revised MM5 Monin-Obukhov scheme.

3.2. Data acquisition and processing

We obtained 2000 and 2010 land use/land cover data from the national land use/land cover database, developed by the Chinese Academy of Sciences and released via the Resource and Environment Data Cloud Platform (http://www.resdc.cn). The land use/land cover data were derived from the Landsat TM/ETM imagery, with a spatial resolution of 1 km × 1 km, and were classified according to the International Geosphere-Biosphere Program (IGBP) land use classification scheme, with an overall classification accuracy of 83.14% (Wu et al., 2013). Here, the 1-km land use/land cover data were aggregated to the inner domain resolution by calculating the dominant land use/land cover type in each 10-km grid cell. The new data sources were subsequently incorporated in the inner domain, and for the outer domain, the default IGBP-Modified MODIS 20-category land use/land cover data, provided by the WRF modeling system, were used.

Vegetation fraction was calculated based on the third generation of GIMMS NDVI (NDVI3g; https://ecocast.arc.nasa.gov/), derived primarily with data from AVHRR sensors at a spatial resolution of 0.083° × 0.083° and temporal resolution of 15 days, following the method proposed by Gutman and Ignatov (1998):

$$FVC = (N - N_s) / (N_v - N_s) \quad (1)$$

where FVC denotes fractional vegetation cover, N the NDVI at each pixel, N_s the bare soil NDVI, and N_v the dense vegetation NDVI. In this work, N_s and N_v were defined as the lower and upper 5% NDVI of the inner domain (Sellers et al., 1997). Leaf area index (LAI) at a spatial resolution of 0.05° × 0.05° and temporal resolution of 8 days was provided by the global land surface satellite (GLASS) products (http://www.geodata.cn/), developed by Beijing Normal University. Field validation indicated that the uncertainty of GLASS LAI was much less than that of MODIS LAI (Xiao et al., 2014). We also calculated blue-sky albedo based on the 30-arc, 8-day global gap-filled, snow-free BRDF parameters product (ftp://rsftp.eeos.umb.edu/). A phenological temporal curve fitting technique was applied to this spatially complete albedo product, so as to fill missing data in the official MOD43B3 product (e.g., not having an observation, being lower quality, or being snow-covered) with geophysically realistic values (Sun et al., 2017). Here, we used white-sky and black-sky albedo obtained from the recently developed BRDF product to calculate blue-sky albedo (Liang et al., 2005):

$$\alpha = f_{dir}\,\alpha_{dir} + f_{dif}\,\alpha_{dif} \quad (2)$$

$$f_{dir} + f_{dif} = 1 \quad (3)$$

where α represents blue-sky albedo, α_{dir} the black-sky albedo, and α_{dif} the white-sky albedo. f_{dir} and f_{dif} are proportions of direct beam and diffuse illumination for total incoming sunlight. The f_{dif} can be estimated as a function of solar zenith angle (Long and Gaustad, 2004). To facilitate use within WRF, the 15-day and 8-day vegetation

characteristics of 2001 and 2010 were linearly interpolated to a daily interval and aggregated to the inner domain resolution (i.e., 10 km) via bilinear interpolation. For the outer domain, vegetation fraction, LAI, and surface albedo from the geographical dataset, provided by the WRF modeling system, were employed.

3.3. Numerical simulation design

We designed two numerical experiments to study the biogeophysical effects of vegetation restoration on regional climate in the Loess Plateau. One signified 2001 landscape (hereafter LP2001) with 2000 land use/land cover data (in replacement of 2001, which was unavailable) and 2001 vegetation characteristics (i.e., vegetation fraction, LAI, and surface albedo). The other signified 2010 landscape (hereafter LP2010) with 2010 land use/land cover data and 2010 vegetation characteristics of the same kinds. The driving meteorology (e.g., 3-d air temperature, wind components, humidity, and pressure; the detailed input meteorological variables required for running WRF can be found in Appendix Table A1) used for all simulations was identical so as to capture the signal of landscape-change-induced forcing. Specifically, each experiment was carried out for five consecutive years, initialized on January 1st, 2000 at 00:00 UTC and terminated on December 31st, 2004 at the same time (Table 2). Output before February 29th, 2000 was considered as spin-up and thus excluded from the following analysis. Note that our study focused on summer (i.e., June, July, and August) because vegetation matures to peak greenness and, thus, exerts the strongest influences on land-atmosphere interactions during this period of year. When illustrating climate effects owing to vegetation changes, all five summers derived from 2000 to 2004 simulations for a particular experiment were averaged and subsequently differentiated.

3.4. Model evaluation data

Observations used for evaluating the performance of the WRF model were derived from the CN05.1 gridded dataset, developed by the National Climate Center of China (http://www.ncc-cma.net). The CN05.1 gridded dataset is produced based on interpolation of meteorological data from about 2400 national weather stations across mainland China, for the purpose of climate model validation (Wu and Gao, 2013). The dataset contains daily and monthly mean meteorological information (e.g., 2-m air temperature and precipitation) covering a period of January 1st, 1961 – December 31st, 2012, with a spatial resolution of 0.25° × 0.25°. To examine the performance of WRF, summer mean 2-m air temperature and precipitation, averaged across all five realizations (i.e., 2000–2004) from LP2001 and LP2010, respectively, were compared with the corresponding averaged gridded observations from the CN05.1 dataset.

We also employed the observation minus reanalysis (OMR; Kalnay and Cai, 2003) approach to help evaluate WRF-simulated summertime 2-m air temperature differences owing to vegetation changes. The data used for the OMR analysis included station-based observations provided by the National Meteorological Information Center of China (http://data.cma.cn/; Wu and Gao, 2013) and the NCEP-DOE Reanalysis II (Kanamitsu et al., 2002). Prior to applying the OMR analysis, the station-based observations were homogenized based on the method of Li and Yan (2009). Summer temperature trends for a time series of 13 years (i.e., 1999–2011) were calculated at each of the station locations within the Loess Plateau using the station-based observations and corresponding gridded reanalysis, respectively. Differences in the trends of temperature variations between those derived from the observations and those derived from the reanalysis can then represent landscape-change-induced temperature changes.

Table 2
Description of all simulations performed.

Simulation	Spin-up period	Analysis time
LP2001	1 Jan 2000 – 29 Feb 2000	1 Mar 2000 – 31 Dec 2004
LP2010	1 Jan 2000 – 29 Feb 2000	1 Mar 2000 – 31 Dec 2004

3.5. Trend detection methods

To help evaluate simulated summertime daytime maximum and nighttime minimum temperature changes, a linear regression model was applied to detect trends of changes in observed summertime maximum and minimum temperature during the period of 1999–2015. A least squares fitting technique was used to calculate the best fitting line for the observed data by minimizing the sum of the squares of the vertical deviations from each data point to the line. The p-value was further calculated to test the significance of the linear regression model. If the p-value was less than 0.05, we deemed that the trends of changes were statistically significant. We also employed this trend detection method to help understand interannual variations in land surface biophysical properties (i.e., NDVI, LAI, and surface albedo) during 2000–2010 in the Loess Plateau, so as to better illustrate vegetation changes due to the GTG program.

3.6. Calculation of surface heat content

While surface air temperature changes are of importance, a concurrent change in low-level moisture content can drop surface heat content (i.e., moist enthalpy) if the air dries even with a positive temperature change, and vice versa. That is, surface air temperature alone does not capture the real change in surface heat content of the Earth system, and the moisture content of surface air must be included (Pielke et al., 2004). Hence, we further calculated modification of surface heat content in the Loess Plateau owing to the GTG program. As proposed by Pielke et al. (2004), the heat content of surface air can be expressed as $H = C_pT + L_vq$, where C_p is the specific heat of air at constant pressure, T the air temperature, L_v the latent heat of vaporization, and q the specific humidity. The quantity, H, is called moist static energy with a unit of J/kg or kJ/kg.

4. Results

4.1. WRF model evaluation

Simulations from LP2001 and LP2010 were evaluated against corresponding gridded observations, respectively, to gauge the performance of the WRF model. Results indicated WRF's capability to reproduce reasonably well the spatial variability of observed 2-m air temperature and precipitation in the Loess Plateau (Fig. 3). In summer, the model properly captured the observed temperature variability, with high temperature simulated in southeastern and northwestern portions of the region, as well as low temperature in western and northeastern parts of the region. The spatial correlation coefficients between the observed and simulated 2-m air temperature were 0.83 for LP2001 and 0.81 for LP2010. In addition, WRF reproduced the observed summer precipitation distribution fairly well, with increased amount of precipitation from the arid to semi-arid to semi-humid areas. The spatial correlation coefficients between the observed and simulated precipitation were 0.70 for LP2001 and 0.72 for LP2010.

Although the WRF model can accurately capture the climatological behavior of the Loess Plateau during the simulated time period, discrepancies inevitably existed between the observations and simulations. For instance, a smaller amount of precipitation was found in southern portions of the region compared with the observed variability. This was likely caused by errors in initial and lateral boundary conditions or intrinsic limitations of WRF. On the other hand, the relatively coarse resolution (i.e., 0.25°) gridded observations may not adequately represent local variability of 2-m air temperature and precipitation

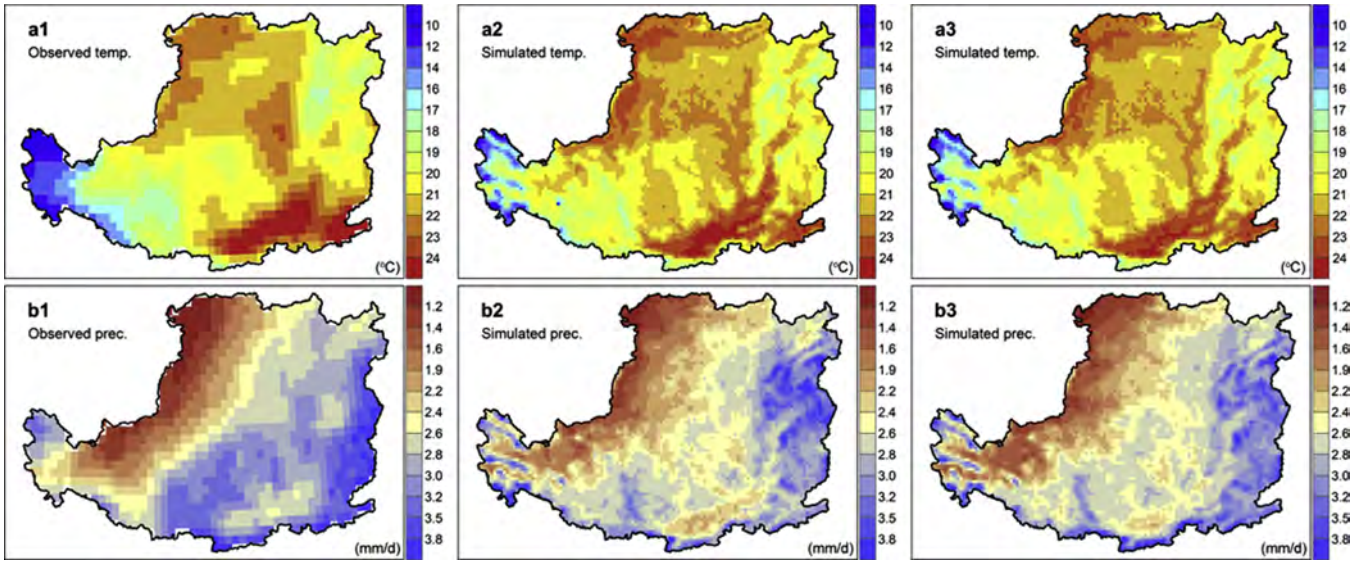

Fig. 3. Observed summer 2-m air temperature (°C) and precipitation (mm/day) in the Loess Plateau (a1 and b1), simulated summer 2-m air temperature and precipitation from LP2001 (a2 and b2), and simulated summer 2-m air temperature and precipitation from LP2010 (a3 and b3). The observed and simulated 2-m air temperature and precipitation were averaged across summers of.2000–2004.

distribution compared with model simulations with a grid spacing of 10 km, especially for near-surface temperature. Such resolution gap may also cause disagreement between observations and simulations.

4.2. Vegetation changes from 2001 to 2010

We first show that the GTG program changed land use/land cover types across the Loess Plateau during 2000–2010 (Fig. 4). As illustrated, the Loess Plateau was dominated by grasslands, croplands, and forests/shrubs, accounting for 41.4%, 36.1%, and 14.0% of the total land areas in 2000, while such proportions were changed to 41.9%, 34.5%, and 14.8% in 2010. The woody plants were mainly distributed in the province of Shanxi, with some scattered in Shaanxi. The grasslands occupied the arid and semi-arid areas, while cultivated lands were spread in the semi-humid areas and along the Yellow River. The barren lands were primarily found in the Mu Us Sandy Land, located in the northwestern part of the region where annual precipitation was generally less than 200 mm. From 2000 to 2010, a considerable portion of farmlands (i.e., 9625 km^2) was removed from the Loess Plateau, thus leading to increments of forests/shrubs (i.e., 5125 km^2) and grasslands (i.e., 3100 km^2). Although the built environment took up a small portion of land areas, rapid expansion of urban lands was notable, particularly in Shanxi and Shaanxi.

Compared with changes in land use/land cover types, modification of land surface biophysical properties was considerably more extensive (Fig. 5). In summer, vegetation fraction and LAI increased while surface

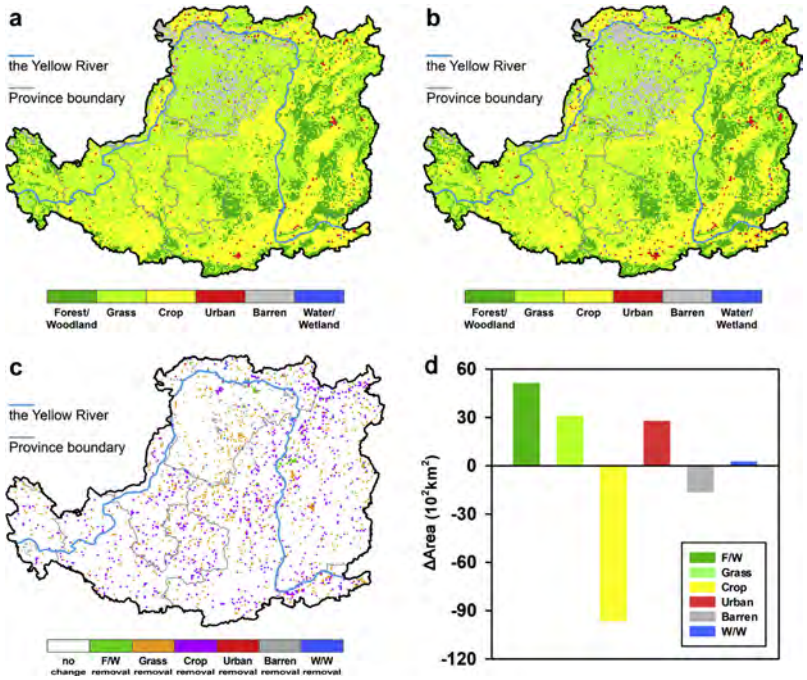

Fig. 4. Spatial pattern of land use/land cover in (a) 2000 and (b) 2010 in the Loess Plateau. Spatial pattern and areas of changes in land use/land cover between 2000 and 2010 are presented in (c) and (d). Note that the legend in (c) indicates the conversion of a certain land use/land cover type to other land use/land cover types.

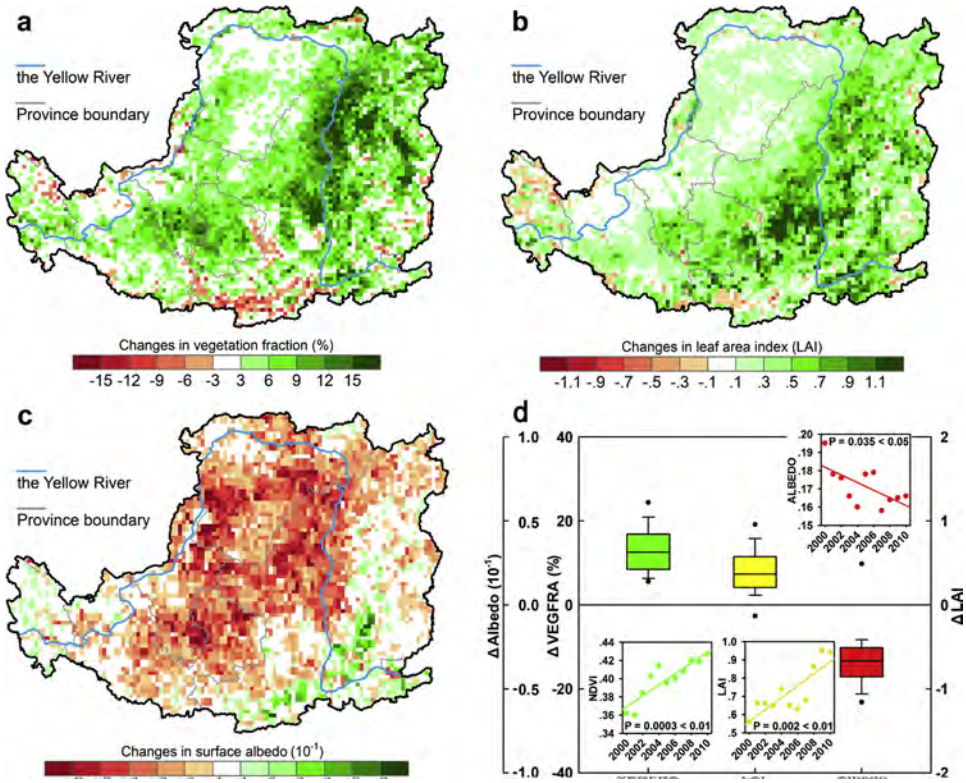

Fig. 5. Spatial pattern of changes in summer (a) vegetation fraction, (b) leaf area index (LAI), and (c) surface albedo from 2001 to 2010 in the Loess Plateau. The box-and-whisker plots of changes in the three parameters with trends of interannual variations in NDVI, LAI, and albedo are illustrated in (d). Across the Loess Plateau, these trends are statistically significant at the 0.01 level for NDVI and LAI and at the 0.05 level for albedo.

albedo decreased in the Loess Plateau. The most apparent increases in vegetation fraction and LAI were found in the provinces of Shanxi and Shaanxi, where the GTG program was first launched dating back to 1999. Maximum increases in vegetation fraction between 15%–20% and LAI between 1.1–1.5 were found in those areas. By contrast, surface albedo was reduced by up to 0.05 – 0.06 in the arid and semi-arid parts. Generally, vegetation fraction increased by 8%–17% and LAI by 0.2 – 0.6, while surface albedo decreased by 0.03 – 0.045 across the Loess Plateau. To further illustrate vegetation changes over time in this part of China, the trends of interannual variations in NDVI, LAI, and surface albedo, averaged across the entirety of Loess Plateau, were calculated using the linear least squares fitting technique. Results indicated that summer mean NDVI and LAI at regional level progressively increased from 2000 to 2010 ($p < 0.01$ for both NDVI and LAI), while the temporal evolution of surface albedo exhibited the opposite trend ($p < 0.05$).

4.3. Changes in 2-m air temperature

Differences in 2-m air temperature between LP2001 and LP2010 exhibited widespread summer cooling in the Loess Plateau (Fig. 6a). The most apparent reduction in daily mean 2-m air temperature was found along the boundary of Shaanxi and Shanxi provinces, with local maximum cooling reaching 0.8 ℃. Scattered warming effects were simulated in the Mu Us Sandy Land (where portions of grasslands were degraded and converted to barren lands) as well as the urbanizing locales. The simulation results generally agreed with the OMR analysis, also indicating non-negligible cooling effects in the eastern half as well as the westernmost part of the region (Fig. 6b). However, prevalent warming signals were detected in Ningxia and Gansu provinces. The discrepancies between the OMR analysis and simulation results were mainly attributed to the high topography of western Loess Plateau (see Fig. 1), which usually decreased the accuracy of the OMR method when applied in mountainous areas. Nevertheless, the agreement between simulated differences in 2-m air temperature and the OMR analysis demonstrated the importance of landscape forcing in modulating thermal conditions of the Loess Plateau.

The reduction of daily mean 2-m air temperature (T_{mean}) was largely ascribed to decreases in nighttime minimum temperature (T_{min}), while changes in daytime maximum temperature (T_{max}) were inconspicuous (Fig. 6c–d). During the daytime, alterations to 2-m air temperature were mostly restricted to 0.4 ℃ except the southeastern part of the region, where T_{max} decreased by 0.4 – 0.7 ℃. In contrast, extensive cooling effects, with the magnitude of 0.8–1.0 ℃, were simulated during the nighttime. Furthermore, dispersed warming effects, on the order of 0.7 – 0.9 ℃, were found in the Mu Us Sandy Land and around 2.0 ℃ in the urbanizing locales. On average, revegetation lowered T_{mean} by 0.15 – 0.4 ℃ for the entire region (Fig. 7). The magnitude of reduction in T_{min} (between 0.2 – 0.5 ℃) was slightly greater than that in T_{mean}, whereas no significant changes in T_{max} were simulated. As a result, the diurnal temperature range (i.e., $T_{max} - T_{min}$) in the Loess Plateau was raised, with the full range of simulated variability between 0.15 – 0.45 ℃.

The comparison of simulated differences in 2-m maximum and minimum temperature with observations can provide additional confidence in the WRF's capability to reproduce the changing summer climate in the Loess Plateau. Consistent with our simulation results, the observed time series of summer daily maximum and minimum temperature during 1999–2015 (we extended the year to 2015 so as to better detect trends of temperature variations) exhibited stronger nighttime relative to daytime cooling (Fig. 8). Note that the two weather stations examined, one in Xi county, Shanxi province and the other in Suide county, Shaanxi province, were both located in areas where the GTG program was first launched in 1999 (Chen et al., 2015). Significant reduction of nighttime minimum temperature was detected in both stations, while changes in daytime maximum temperature displayed more fluctuation. This was especially true for the station in Xi county, Shanxi province, where significant ($p \approx 0 < 0.01$) and sharp decreases (1.0 ℃/10 yr, which was close to our simulation results) in nighttime minimum temperature but no significant changes ($p = 0.21 > 0.05$) in daytime maximum temperature were calculated.

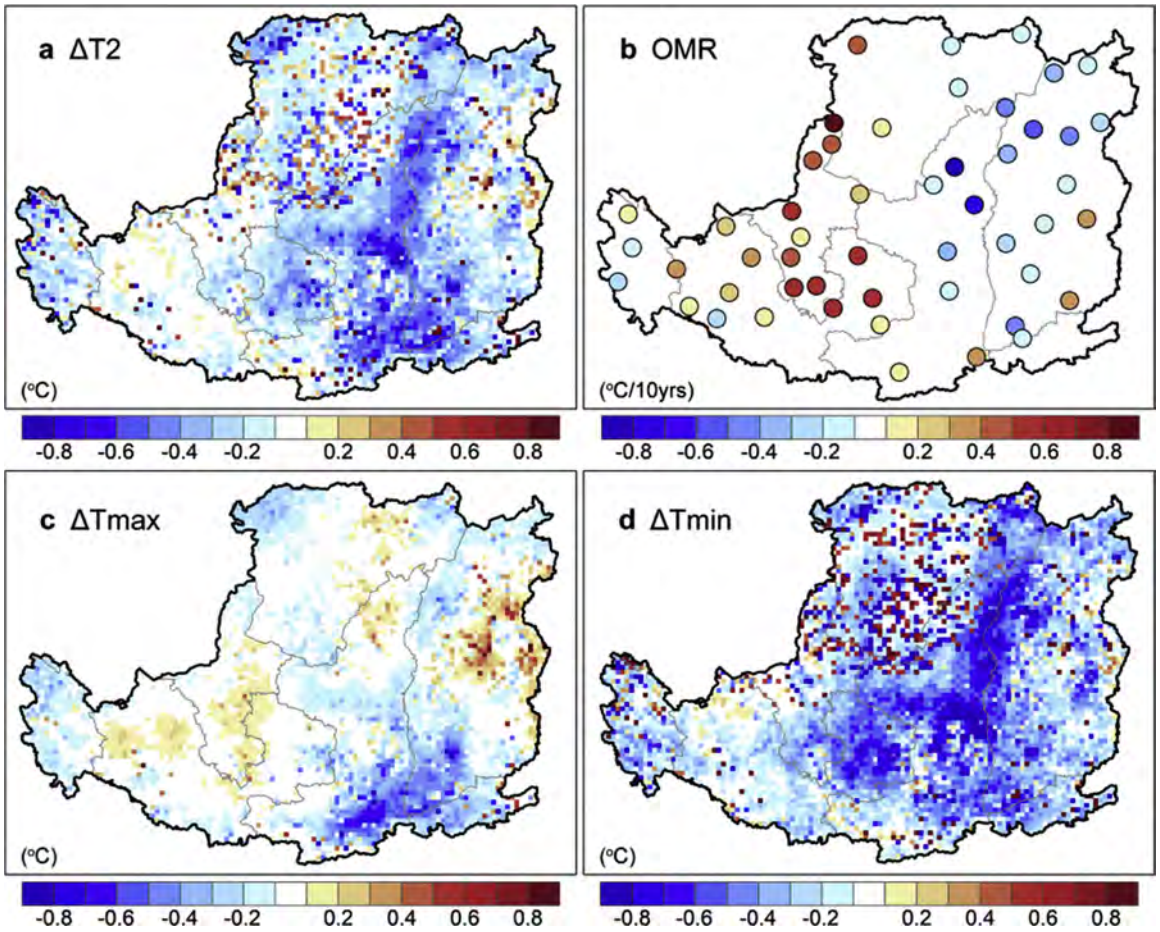

Fig. 6. Spatial pattern of simulated differences (LP2010 – LP2001) in summer daily mean 2-m air temperature (a; °C), decadal trends of summer 2-m air temperature during the period of 1999–2011 at meteorological stations within the Loess Plateau (b; °C/decade), and spatial pattern of simulated differences in summer daytime maximum and nighttime minimum temperature (c and d; °C).

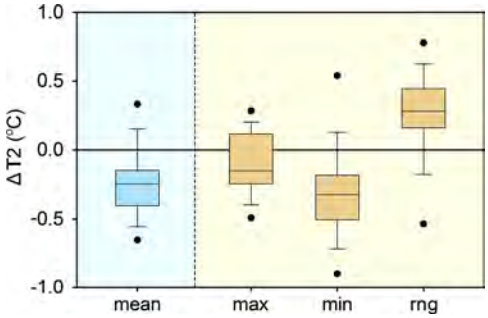

Fig. 7. Box-and-whisker plots of simulated differences (LP2010 – LP2001) in summer daily mean, daytime maximum, nighttime minimum, and diurnal temperature range (T_{rng} = T_{max} – T_{min}) across the Loess Plateau.

4.4. Changes in surface energy budget

We further examined modification of daytime and nighttime surface energy budget to give insights into the physical drivers of 2-m air temperature changes presented earlier (Fig. 9). As expected, the spatial pattern of changes in daytime surface net radiation flux exhibited considerable similarity to that of changes in surface albedo. In areas where the albedo was reduced, the net radiation flux increased accordingly, and vice versa. Overall, increases of 5–25 W/m^2 in daytime surface net radiation flux were simulated for the majority of locales in the Loess Plateau. Modification of surface radiation flux, along with changes in vegetation characteristics (e.g., vegetation fraction and LAI), further resulted in alterations to surface energy budget.

During the daytime, decreases in sensible heat flux and extensive increases in latent heat flux, on the order of 30–35 W/m^2, were simulated in areas with substantial increments of greenness. Meanwhile, ground heat flux was reduced by 5–15 W/m^2 on average in those areas

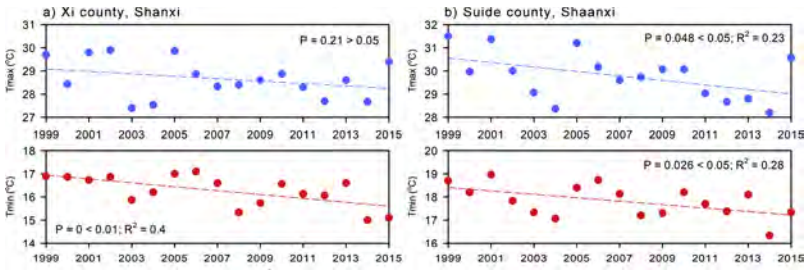

Fig. 8. Observed time series of summer daytime maximum (blue dots) and nighttime minimum (red dots) temperature during the period of 1999–2015 at meteorological stations in (a) Xi county, Shanxi province (36.7 °N, 110.95 °E) and (b) Suide county, Shaanxi province (37.5 °N, 110.2 °E). The straight lines represent trends of the time series using a linear least squares fitting technique (For interpretation of the references to colour in this figure legend, the reader is referred to the web version of this article).

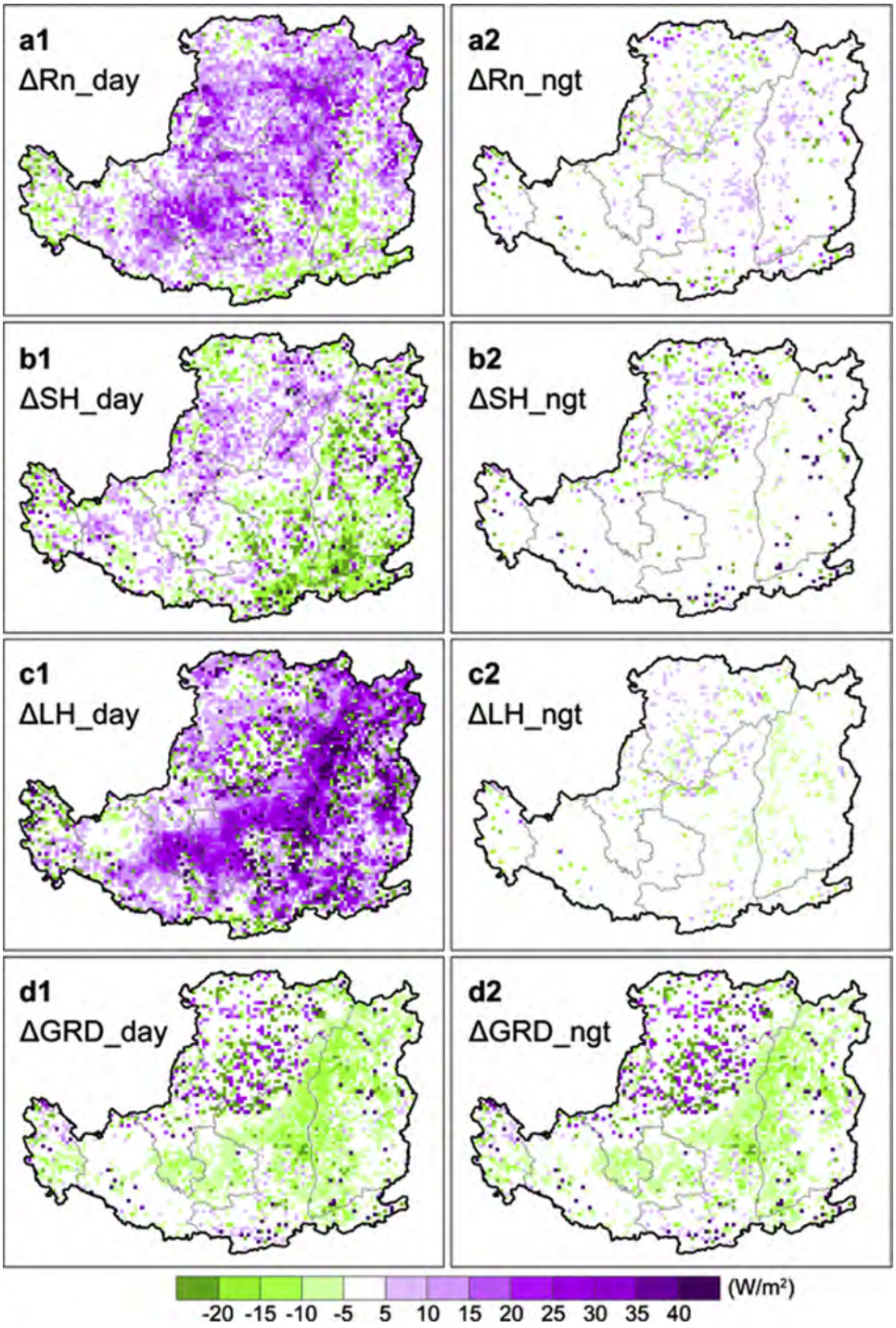

Fig. 9. Spatial pattern of simulated differences (LP2010 – LP2001) in summer daytime (00:00 and 06:00 UTC, i.e., 08:00 and 14:00 LST) and nighttime (12:00 and 18:00 UTC, i.e., 20:00 and 02:00 LST) mean net radiation flux (a1 and a2; Rn), sensible heat flux (b1 and b2; SH), latent heat flux (c1 and c2; LH), and ground heat flux (d1 and d2; GRD). Note that the negative ΔGRD in the daytime indicates the reduction of energy storage in the ground, while the negative ΔGRD in the nighttime signifies the reduction of energy release from the ground. Unit: W/m^2.

while increasing by 15–25 W/m^2 in the locales of northwestern Loess Plateau (i.e., the Mu Us Sandy Land). Here, the negative changes in daytime ground heat flux meant that the downwelling solar energy stored in the ground was reduced, and vice versa. During the nighttime, changes in surface net radiation, sensible heat, and latent heat fluxes were minimal, generally less than 10 W/m^2. However, ground heat flux decreased with a similar order of magnitude as it did during the daytime, indicating the reduction of energy release from the ground at night.

4.5. Changes in 2-m moisture and heat content

In addition to 2-m air temperature, we also analyzed changes in near-surface humidity to help assess the heat content of surface air. As shown in Fig. 10a, simulated differences (LP2010 – LP2001) in 2-m water vapor mixing ratio indicated widespread reduction of low-level moisture content over the Loess Plateau, on the order of 0.1 – 0.4 g/kg in general. Minimal changes were simulated in the well revegetated areas, although a small portion of increases in moisture content,

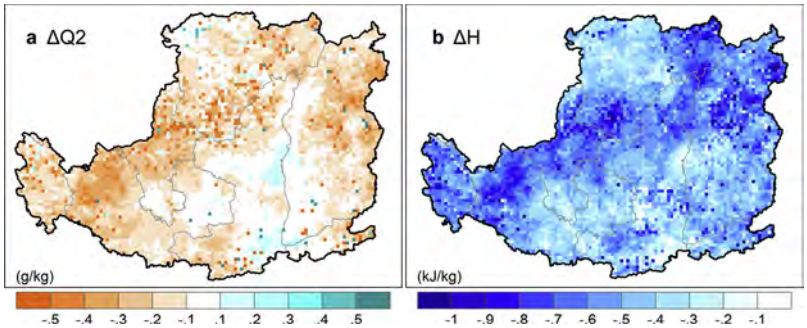

Fig. 10. Spatial pattern of simulated differences (LP2010 – LP2001) in summer 2-m water vapor mixing ratio (a; Q2) and heat content (b; H). Unit: g/kg and kJ/kg.

between 0.1 – 0.2 g/kg, was found in the province of Shaanxi. The concurrent modification of 2-m specific humidity and air temperature, can further enhance or weaken near-surface heat content (i.e., moist enthalpy). Notably, the concurrent decreases in 2-m specific humidity and air temperature led to widespread reduction of near-surface heat content in the Loess Plateau (Fig. 10b). Throughout the region, the majority of locales had the heat content decreased by 0.3 – 0.5 kJ/kg, while local maximum decreases in heat content can range between 0.7–1.0 kJ/kg. That is, drier and cooler weather conditions as a result of vegetation changes were anticipated for people living and working in the Loess Plateau during the summer.

4.6. Changes in precipitation

Simulated differences (i.e., LP2010 – LP2001) in summer precipitation indicated that vegetation restoration affected the hydrometeorological conditions of the Loess Plateau. The most pronounced decrease in summer precipitation occurred in western Loess Plateau and northern Shanxi province, with local maximum reduction on the order of 1.0–1.4 mm/day (Fig. 11a). Notable increases in summer precipitation of 1.0–2.0 mm/day were found in southeastern Loess Plateau. These changes were statistically significant at the 0.05 level (i.e., $P = 0.018 < 0.05$). Fragmented changes in summer precipitation, no more than 1.0 mm/day, were simulated in other parts of the region. In addition to the absolute amount, the percentage change in summer precipitation (i.e., (LP2010 – LP2001)/LP2001) was also examined (Fig. 11b). We found that for areas having relatively small changes in the amount of precipitation, the percentage change in precipitation was not trivial, particularly for the arid areas. Once again, southeastern Loess Plateau displayed the largest increases in the percentage change in summer precipitation (i.e., 20%–40%), while the western portions of the region had the highest decreases in that (i.e., 10%–30%).

We further calculated the frequency histogram of simulated summer accumulated precipitation so as to assess the effects of vegetation restoration on the distribution of precipitation intensity in the Loess Plateau (Fig. 11c). Results indicated that landscape changes from 2001 to 2010 increased summer accumulated precipitation between 300–360 mm while reducing that between 180–300 mm. It should be noted that the areas having the amount of precipitation falling into 180–360 mm accounted for ~ 50% of the total land mass of the Loess Plateau. In addition, vegetation changes tended to inhibit high (i.e., > 600 mm) and low (i.e., 60–120 mm) accumulation of precipitation. Differences in the distribution of precipitation intensity can also help understand, though to some extent, modification of extreme precipitation.

5. Discussion

5.1. Impacts of vegetation restoration on regional climate

This study characterized the spatiotemporal pattern of regional climate change owing to vegetation restoration in the Loess Plateau, through assessment of appropriate climate metrics (e.g., 2-m air temperature, surface energy budget components, humidity, and precipitation). Compared with previous research using qualitative methods (e.g., Fan et al., 2015a,b), our modeling work made a first systematic effort to simulate the complex biogeophysical feedback of revegetation to regional climate and to provide quantitative assessment of how, and to what extent, climate conditions in the Loess Plateau were affected by the China's largest ecological restoration program ever implemented. Results illustrated that 2-m air temperature decreased in summer months, with the magnitude of reduction in nighttime minimum greater than that in daytime maximum. The concurrent decrease in low-level atmospheric moisture content further gave rise to widespread reduction of surface air heat content (i.e., moist enthalpy), thus creating drier and cooler environments in summer for people residing in this part of China.

The landscape-change-induced 2-m air temperature change was largely determined by changes in surface turbulent heat fluxes. On a daily scale, it seemed that the reduction of Bowen ratio due to decreased sensible heat and increased latent heat fluxes contributed to near-surface cooling in the Loess Plateau. However, that was not the case when considering daytime and nighttime surface energy budget separately. In the daytime, the reduction of Bowen ratio did not necessarily lead to notable decreases in 2-m air temperature, because considerable surface heat fluxes were transported to the overlying atmosphere. Such effects were enhanced in our case when a large portion of the Loess Plateau underwent increased planetary boundary layer (PBL) height during the daytime (see Appendix Fig. A1). However, changes in daytime ground heat flux can directly affect nighttime temperature (Zhou et al., 2007). As the latent heat flux largely increased in the daytime, the soil heat storage was reduced accordingly. Thus, less energy was released from the ground to heat the low-level atmosphere in the nighttime. Along with the much lower and decreased PBL depth, the nighttime temperature was reduced substantially.

Our simulation results in terms of changes in daytime and nighttime temperature were generally consistent with observed data, although the observations integrated variations in both land surface and background climate conditions. Our study was also comparable with a prior study reporting much stronger negative effects of vegetation dynamics on nighttime minimum temperature than on daytime maximum temperature in northern China (Wu et al., 2011). However, Peng et al. (2014) found that afforestation may lower daytime land surface temperature (LST) while raising nighttime LST in northern China. It was supposed that the daytime cooling in areas where the decreased or slightly increased evapotranspiration cannot cancel the extra absorbed solar energy of planted forests (as revealed by satellite data) was attributed to the higher efficiency of convective heat transport due to increases in sensible heat flux. This work provided enlightenment for our study as Peng et al. (2014) acknowledged that future research should employ coupled land-atmosphere models to better understand the physical drivers of temperature changes induced by afforestation. Although the

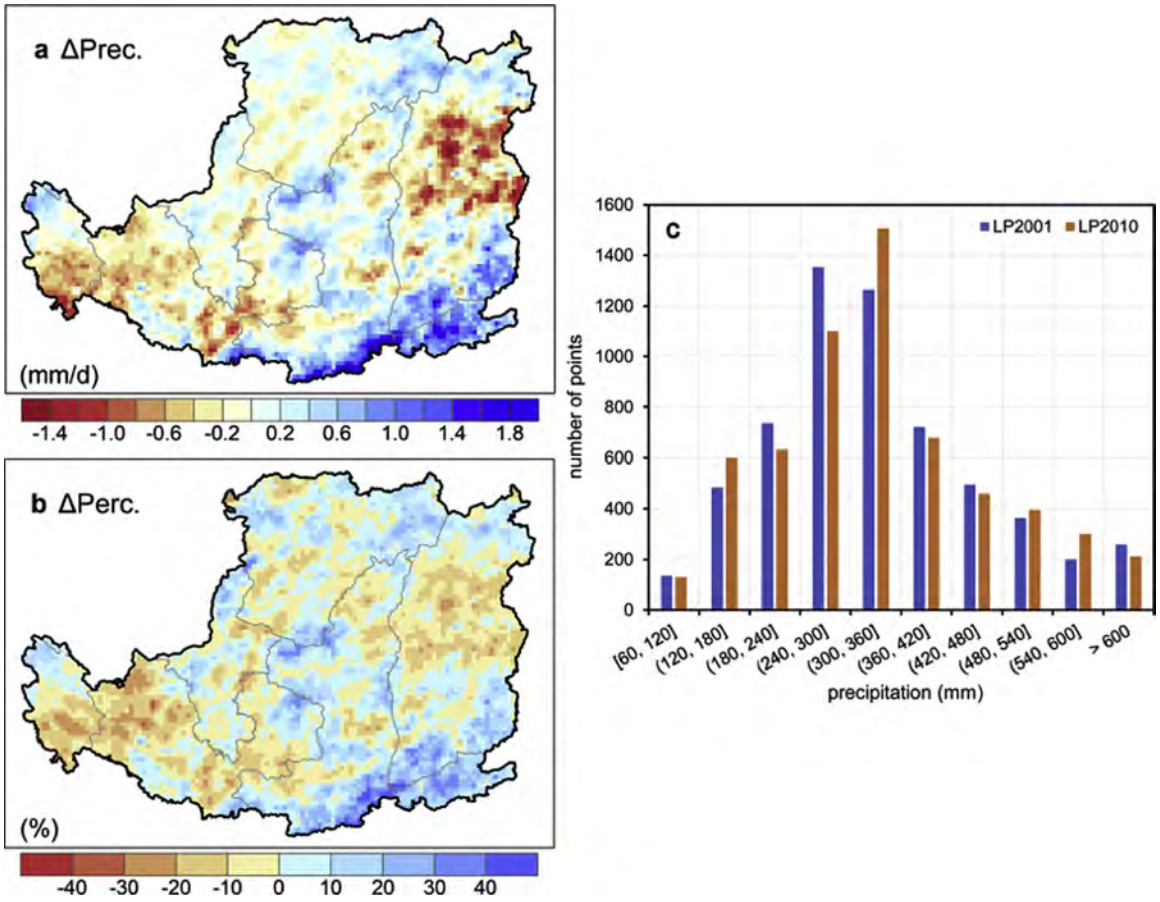

Fig. 11. Spatial pattern of simulated differences (a LP2010 – LP2001; mm/day) and percentage changes (b (LP2010 – LP2001)/LP2001; %) in summer precipitation over the Loess Plateau. Also shown is the frequency histogram of simulated summer accumulated precipitation distribution derived from LP2001 and LP2010 (c; mm).

method, the material, and the scale of analysis used can make the difference, this stimulates our attention that modeling-based work is necessary for the better understanding of land-atmosphere interactions.

In addition to 2-m air temperature, our study also assessed the effects of vegetation restoration on near-surface humidity, which were seldom examined in relevant research (Peng et al., 2014; Fan et al., 2015b; Li et al., 2015). Unexpectedly, although changes in low-level atmospheric moisture content coincided with changes in latent heat flux (i.e., more increases in latent heat flux will result in less decreases in moisture content, and vice versa), 2-m water vapor underwent minimal changes in areas where considerable increments of vegetation greenness were monitored. This was partly because of the climate regime of the Loess Plateau. For a semi-arid region, the moisture content in the air and soil was relatively low. That is, although revegetation can enhance evapotranspiration to some extent, the humidity will not change that much. Together with the transport of low-level moisture content to the overlying atmosphere, changes in 2-m water vapor were therefore trivial. For areas with almost no changes in greenness, the decrease or small increase in latent heat flux with enhanced convective transport led to obvious reduction of 2-m water vapor. It should be noted that advective moisture transport may also play a role in modification of low-level moisture content.

Compared with changes in 2-m air temperature and humidity, changes in precipitation owing to the GTG program exhibited large spatial variability. Indeed, precipitation changes were not only affected by regional evapotranspiration but also large-scale dynamics. Under the background of global climate change, the total amount of precipitation on wet days exhibited declining trends in most parts of the Loess Plateau during 1961–2010 (Wang et al., 2012; Sun et al., 2015). Similar with our simulation results, the most pronounced observed decreases in precipitation were found in Shanxi and Gansu provinces (Wang et al., 2012; Sun et al., 2015). Such consistency can at least illustrate that vegetation changes played a part in the hydrometeorological behavior of the Loess Plateau. However, it should also be acknowledged that the mechanism of precipitation changes was complicated and beyond the scope of our study (we mainly focused on near-surface climate metrics). Future research should analyze the physical drivers of precipitation changes in the case of realistic landscape changes. This is particularly meaningful for the arid and semi-arid areas like the Loess Plateau, where the water resource is a limiting factor for the survival of people and thus regional sustainable development.

5.2. Implications for the GTG program

To date, the GTG program has been launched for nearly 20 years and the total amount of investment in the program will reach a new level (i.e., 64.9 billion USD) by 2050 (Feng et al., 2016). Hence, it's time for a comprehensive assessment of the environmental outcomes of the GTG program, so as to better guide the follow-up investment. Unlike previous research targeted on ecosystem services (e.g., Feng et al., 2013; Su and Fu, 2013; Li et al., 2016; Wang et al., 2016), our study examined the effects of the GTG program from a regional climate change perspective. We found that although the ecological restoration program lowered near-surface temperature considerably, it did not play a positive role in the improvement of the hydrometeorological conditions in the Loess Plateau. What's worse, enhanced evapotranspiration of the newly planted trees may reduce soil moisture and surface runoff, thus exacerbating water shortage in afforested areas (Cao et al., 2009;

Feng et al., 2016). An alternative approach is to restore native vegetation (be it trees, shrubs, or grasses) with reasonable extent, rather than large-scale afforestation in water-deficient areas (which usually leads to low survival rates). Indeed, the restoration of overgrazed lands and the removal of farmlands in marginal areas have the largest effects on vegetation recovery in arid and semiarid regions like the Loess Plateau (Cao et al., 2009).

6. Conclusions

The GTG program has been implemented for almost 20 years, and examining its regional climate effects is important for improving regional environmental policy. This study, using of a coupled land-atmosphere model, established a first process-based, quantitative assessment of how, and to what extent, vegetation changes owing to the GTG program affected summer climate in the Loess Plateau, the largest loessal area of the world. From 2001 to 2010, a large number of croplands were converted to forests/shrubs and grasslands, with vegetation fraction and LAI increasing and surface albedo decreasing in the region. As a result, 2-m air temperature was reduced, with the magnitude of reduction in nighttime minimum greater than daytime maximum. The concurrent decrease in 2-m specific humidity further led to widespread reduction of near-surface heat content (i.e., moist enthalpy). In addition, precipitation decreased in northern Shanxi province and western Loess Plateau while increasing in southeastern Loess Plateau. Our findings highlight the substantial impacts of vegetation changes on regional climate and have critical implications (e.g., to restore native vegetation with reasonable extent) for the sustainable practice of the GTG program.

Competing interests

The authors declare no competing interests.

Acknowledgements

This study was supported by the Fund for Creative Research Groups of the National Natural Science Foundation of China (41621061), the National Natural Science Foundation of China (41801179), the China Postdoctoral Science Foundation (2017M620664), and the National Basic Research Program of China (2014CB954301).

Appendix A

Table A1
Required meteorological fields for running WRF.

Field name	Units	Description
TT	K	3-d temperature
RH	%	3-d relative humidity
SPECHUMD	kg/kg	3-d specific humidity
UU	m/s	3-d wind u-component
VV	m/s	3-d wind v-component
GHT	m	3-d geopotential height
PRESSURE	Pa	3-d pressure
PSFC	Pa	Surface pressure
PMSL	Pa	Mean sea-level pressure
SKINTEMP	K	Skin temperature
SOILHGT	m	Soil height
TT	K	2-m air temperature
RH	%	2-m relative humidity
SPECHUMD	kg/kg	2-m specific humidity
UU	m/s	2-m wind u-component
VV	m/s	2-m wind v-component
LANDSEA	fraction	Land-sea mask
SM*tttbbb*[a]	m^3/m^3	Soil moisture
ST*tttbbb*	K	Soil temperature
SOILM*mmm*[b]	kg/m^3	Soil moisture
SOILT*mmm*	K	Soil temperature

[a] '*ttt*' is the layer top depth in cm, and '*bbb*' is the layer bottom depth in cm.
[b] '*mmm*' is the level depth in cm.

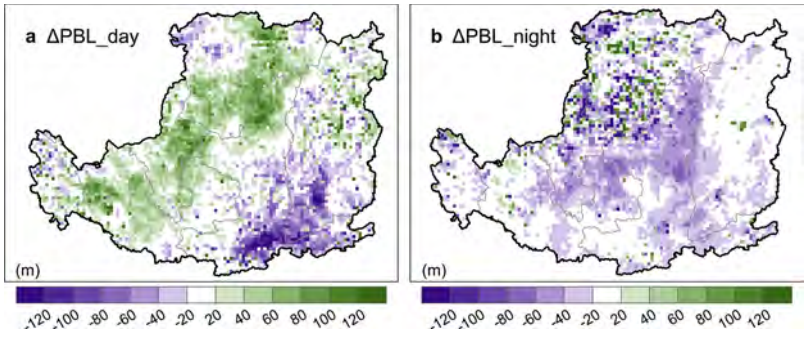

Fig. A1. Spatial pattern of simulated differences (LP2010 – LP2001) in summer (a) daytime and (b) nighttime planetary boundary layer (PBL) height. Unit: m.

References

Bryan, B.A., Gao, L., Ye, Y., Sun, X., Connor, J.D., Crossman, N.D., Stafford-Smith, M., Wu, J., He, C., Yu, D., Liu, Z., Li, A., Huang, Q., Ren, H., Deng, X., Zheng, H., Niu, J., Han, G., Hou, X., 2018. China's response to a national land-system sustainability emergency. Nature 559, 193–204.

Cao, S., Chen, L., Yu, X., 2009. Impact of China's Grain for Green Project on the landscape of vulnerable arid and semi-arid agricultural regions: a case study in northern Shaanxi Province. J. Appl. Ecol. 46, 536–543.

Cao, Q., Yu, D., Georgescu, M., Han, Z., Wu, J., 2015. Impacts of land use and land cover change on regional climate: a case study in the agro-pastoral transitional zone of China. Environ. Res. Lett. 10, 124025.

Chen, F., Dudhia, J., 2001. Coupling an advanced land surface-hydrology model with the Penn State-NCAR MM5 modeling system. Part I: model implementation and sensitivity. Mon. Weather Rev 129, 569–585.

Chen, Y., Wang, K., Lin, Y., Shi, W., Song, Y., He, X., 2015. Balancing green and grain trade. Nat. Geosci. 8, 739–741.

Fan, X., Ma, Z., Yang, Q., Han, Y., Mahmood, R., Zheng, Z., 2015a. Land use/land cover changes and regional climate over the Loess Plateau during 2001-2009. Part I: observational evidence. Clim. Change 129, 427–440.

Fan, X., Ma, Z., Yang, Q., Han, Y., Mahmood, R., 2015b. Land use/land cover changes and regional climate over the Loess Plateau during 2001-2009. Part II: interrelationship from observations. Clim. Change 129, 441–455.

Feddema, J.J., Oleson, K.W., Bonan, G.B., Mearns, L.O., Buja, L.E., Meehl, G.A., Washington, W.M., 2005. The importance of land-cover change in simulating future climates. Science 310, 1674–1678.

Feng, X., Fu, B., Lu, N., Zeng, Y., Wu, B., 2013. How ecological restoration alters ecosystem services: an analysis of carbon sequestration in China's Loess Plateau. Sci. Rep. 3, 2846.

Feng, X., Fu, B., Piao, S., Wang, S., Ciais, P., Zeng, Z., Lü, Y., Zeng, Y., Li, Y., Jiang, X., Wu, B., 2016. Revegetation in China's Loess Plateau is approaching sustainable water resource limits. Nat. Clim. Change 6, 1019–1022.

Foley, J.A., DeFries, R., Asner, G.P., Barford, C., Bonan, G., Carpenter, S.R., Chapin, F.S., Coe, M.T., Daily, G.C., Gibbs, H.K., Helkowski, J.H., Holloway, T., Howard, E.A., Kucharik, C.J., Monfreda, C., Patz, J.A., Prentice, I.C., Ramankutty, N., Snyder, P.K., 2005. Global consequences of land use. Science 309, 570–574.

Georgescu, M., Morefield, P.E., Bierwagen, B.G., Weaver, C.P., 2014. Urban adaptation can roll back warming of emerging megapolitan regions. Proc. Natl. Acad. Sci. U. S. A. 111, 2909–2914.

Gutman, G., Ignatov, A., 1998. The derivation of the green vegetation fraction from NOAA/AVHRR data for use in numerical weather prediction models. Int. J. Remote Sens. 19, 1533–1543.

Kalnay, E., Cai, M., 2003. Impact of urbanization and land-use change on climate. Nature 423, 528–531.

Kanamitsu, M., Ebisuzaki, W., Woollen, J., Shi-Keng, Y., 2002. NCEP-DOE AMIP-II reanalysis (R-2). Bull. Am. Meteorol. Soc. 83, 1631–1643.

Li, Z., Yan, Z., 2009. Homogenized daily mean/maximum/minimum temperature series for China from 1960-2008. Atmos. Ocean. Sci. Lett. 2, 237–243.

Li, Z., Liu, X., Niu, T., Kejia, D., Zhou, Q., Ma, T., Gao, Y., 2015. Ecological restoration and its effects on a regional climate: the source region of the Yellow River, China. Environ. Sci. Technol. 49, 5897–5904.

Li, S., Liang, W., Fu, B., Lü, Y., Fu, S., Wang, S., Su, H., 2016. Vegetation changes in recent large-scale ecological restoration projects and subsequent impact on water resources in China's Loess Plateau. Sci. Total Environ. 569, 1032–1039.

Li, J., Peng, S., Li, Z., 2017. Detecting and attributing vegetation changes on China's Loess Plateau. Agric. Forest Meteorol. 247, 260–270.

Liang, X., Xu, M., Gao, W., Kunkel, K., Slusser, J., Dai, Y., Min, Q., Houser, P.R., Rodell, M., Schaaf, C.B., Gao, F., 2005. Development of land surface albedo parameterization based on moderate resolution imaging spectroradiometer (MODIS) data. J. Geophys. Res. Atmos. 110, D11107.

Liu, G., Shang-Guan, Z., Yao, W., Yang, Q., Zhao, M., Dang, X., Guo, M., Wang, G., Wang, B., 2017. Ecological effects of soil conservation in Loess Plateau. Bull. Chin. Acad. Sci. 32, 11–19.

Long, C., Gaustad, K., 2004. The Shortwave (SW) Clear-Sky Detection and Fitting Algorithm: Algorithm Operational Details and Explanations. Pacific Northwest National Laboratory.

Peng, S., Piao, S., Zeng, Z., Ciais, P., Zhou, L., Li, L.Z.X., Myneni, R.B., Yin, Y., Zeng, H., 2014. Afforestation in China cools local land surface temperature. Proc. Natl. Acad. Sci. U. S. A. 111, 2915–2919.

Pielke, R.A., 2005. Land use and climate change. Science 310, 1625–1626.

Pielke, R.A., Niyogi, D., 2009. The role of landscape processes within the climate system. In: Otto, J.C., Dikau, R. (Eds.), Landform-Structure, Evolution, Process Control. Springer-Verlag, Berlin Heidelberg, pp. 67–85.

Pielke, R.A., Davey, C., Morgan, J., 2004. Assessing "global warming" with surface heat content. Eos. Trans. AGU 85, 210–211.

Pielke, R.A., Pitman, A., Niyogi, D., Mahmood, R., McAlpine, C., Hossain, F., Klein Goldewijk, K., Nair, U., Betts, R., Fall, S., Reichstein, M., Kabat, P., de Noblet, N., 2011. Land use/land cover changes and climate: modeling analysis and observational evidence. WIRES Clim. Chang. 2, 828–850.

Pitman, A.J., de Noblet-Ducoudré, N., Avila, F.B., Alexander, L.V., Boisier, J.P., Brovkin, V., Delire, C., Cruz, F., Donat, M.G., Gayler, V., van den Hurk, B., Reick, C., Voldoire, A., 2012. Effects of land cover change on temperature and rainfall extremes in multi-model ensemble simulations. Earth Syst. Dynam. 3, 213–231.

Sellers, P.J., Dickinson, R.E., Randall, D.A., Betts, A.K., Hall, F.G., Berry, J.A., Collatz, G.J., Denning, A.S., Mooney, H.A., Nobre, C.A., Sato, N., Field, C.B., Henderson-Sellers, A., 1997. Modeling the exchanges of energy, water, and carbon between continents and the atmosphere. Science 275, 502–509.

Shang, X., Li, X., 2010. Holocene vegetation characteristics of the southern Loess Plateau in the Weihe River valley in China. Rev. Palaeobot. Palyno. 160, 46–52.

Skamarock, W.C., Klemp, J.B., Dudhia, J., Gill, D.O., Barker, D.M., Wang, W., Powers, J.G., 2008. A Description of the Advanced Research WRF Version 3 (No. NCAR/TN-475 + STR). NCAR Technical Note. https://doi.org/10.5065/D68S4MVH.

Su, C., Fu, B., 2013. Evolution of ecosystem services in the Chinese Loess Plateau under climatic and land use changes. Global Planet. Change 101, 119–128.

Sun, Q., Miao, C., Duan, Q., Wang, Y., 2015. Temperature and precipitation changes over the Loess Plateau between 1961 and 2011, based on high-density gauge observations. Global Planet. Change 132, 1–10.

Sun, Q., Wang, Z., Li, Z., Erb, A., Schaaf, C.B., 2017. Evaluation of the global MODIS 30 arc-second spatially and temporally complete snow-free land surface albedo and reflectance anisotropy dataset. Int. J. Appl. Earth Obs. 58, 36–49.

Wang, T., Wu, J., Kou, X., Oliver, C., Mou, P., Ge, J., 2010. Ecologically asynchronous agricultural practice erodes sustainability of the Loess Plateau of China. Ecol. Appl. 20, 1126–1135.

Wang, Q., Fan, X., Qin, Z., Wang, M., 2012. Change trends of temperature and precipitation in the Loess Plateau Region of China, 1961-2010. Global Planet. Change 92, 138–147.

Wang, S., Fu, B., Piao, S., Lü, Y., Ciais, P., Feng, X., Wang, Y., 2016. Reduced sediment transport in the Yellow River due to anthropogenic changes. Nat. Geosci. 9, 38–41.

Wang, L., Cheung, K.K., Tam, C.Y., Tai, A.P., Li, Y., 2018. Evaluation of the regional climate model over the Loess Plateau of China. Int. J. Climatol. 38, 35–54.

Wu, J., Gao, X., 2013. A gridded daily observation dataset over China region and comparison with the other datasets. Chin. J. Geophys. 56, 1102–1111 (In Chinese).

Wu, L., Zhang, J., Dong, W., 2011. Vegetation effects on mean daily maximum and minimum surface air temperatures over China. Chin. Sci. Bull. 56, 900–905.

Wu, F., Zhan, J., Yan, H., Shi, C., Huang, J., 2013. Land cover mapping based on multisource spatial data mining approach for climate simulation: a case study in the farming-pastoral ecotone of North China. Adv. Meteorol. 2013, 520803.

Xiao, J., 2014. Satellite evidence for significant biophysical consequences of the "Grain for Green" Program on the Loess Plateau in China. J. Geophys. Res. Biogeo. 119, 2261–2275.

Xiao, Z., Liang, S., Wang, J., Chen, P., Yin, X., Zhang, L., Song, J., 2014. Use of general regression neural networks for generating the GLASS leaf area index product from timeseries MODIS surface reflectance. IEEE T. Geosci. Remote 52, 209–223.

Zhai, J., Liu, R., Liu, J., Huang, L., Qin, Y., 2015. Human-induced landcover changes drive a diminution of land surface albedo in the Loess Plateau (China). Remote Sens. 7, 2926–2941.

Zheng, Y., Alapaty, K., Herwehe, J.A., Del Genio, A.D., Niyogi, D., 2016. Improving high-resolution weather forecasts using the Weather Research and Forecasting (WRF) Model with an updated Kain-Fritsch scheme. Mon. Weather Rev. 144, 833–860.

Zhou, L., Dickinson, R.E., Tian, Y., Vose, R.S., Dai, Y., 2007. Impact of vegetation removal and soil aridation on diurnal temperature range in a semiarid region: application to the Sahel. Proc. Natl. Acad. Sci. U. S. A. 104, 17937–17942.